J Mater Sci (2009) 44:6325–6332
DOI 10.1007/s10853-009-3871-3

Nanostructure characterization of polymer-stabilized gold nanoparticles and nanofilms derived from green synthesis

Iliana Medina-Ramírez · Maribel González-García · Jingbo Louise Liu

Received: 16 May 2009 / Accepted: 9 September 2009 / Published online: 23 September 2009

Abstract The fabrication and characterization of gold (Au) nanostructured materials draws significant attention because of their distinctive properties and their technological applications. The first objective of this study is to fabricate polymer-stabilized Au nanoparticles and nanofilms (PAN) through a cost effective and green synthetic methodology. In this study, the gold trication (Au^{3+}) can be spontaneously converted into metallic gold atom using a non-toxic reductant (ascorbic acid). The ultrafine Au clusters were formed and stabilized through metallic bonds in the colloidal suspension, which was then deposited on a micro-glass or polymer-bead substrate to prepare thin films. It was found that ascorbic acid was the best reducing agent due to its rapid rate, spontaneity of reaction, and its non-toxic nature. In order to prevent aggregation of the nanoparticles, a dispersing agent (gum Arabic) was used. The second objective of this study was to analyze the PAN using a number of state-of-the-art instrumentation techniques and analytical approaches, such as X-ray powder diffraction (XRD), atomic force microscopy (AFM), scanning and transmission electron microscopy (SEM and TEM), ultraviolet–visible (UV–Vis) spectroscopy, and ZetaPALS. These techniques were applied to evaluate specific properties of the PAN, such as characterization of its crystalline phase, surface topology, characteristic plasmon, particle size distribution, and stability. From this study, it can be concluded that the ultrafine Au nanoparticles and uniform films were obtained using the green chemistry method. The ultrafine Au particles are highly stabilized and monodispersed as demonstrated by their high absolute value of zeta potential.

Abbreviations

Au	Gold
GA	Gum arabic
NPs	Nanoparticles
PAN	Polymer-stabilized Au nanoparticle and nanofilm
XRD	X-ray powder diffraction
AFM	Atomic force microscopy
SEM	Scanning electron microscopy
TEM	Transmission electron microscopy
EDS	X-ray energy dispersive spectroscopy
UV–Vis	Ultraviolet visible spectroscopy

Introduction

Nanoscale science and technology are inherently multidisciplinary fields, which have drawn significant attention due to their uses in a diverse range of applications, such as electronics, nanomechanics, sensors and actuators, water and air purification, green energy resources, drug delivery, cancer diagnosis, and medicine [1–3]. The term nanotechnology was popularized by Drexler [4, 5] who described the ability to build products by molecular manufacturing. The fundamental objective of using a nanotechnological approach is to manufacture, control, design, and study nanostructures and nanodevices with dimensions of less than 100 nm [6–8]. Engineered nanomaterials have different

I. Medina-Ramírez
Department of Chemistry, Universidad Autónoma de Aguascalientes, Av. Universidad 940, C.P. 20100 Aguascalientes, Mexico

M. González-García · J. L. Liu (✉)
Department of Chemistry, Texas A&M University-Kingsville, MSC 161, 700 University Blvd., Kingsville, TX 78363-8202, USA
e-mail: Jingbo.liu@tamuk.edu; kfjll00@tamuk.edu

properties relative to their macroscale counterparts and thus can be used, for instance, as building blocks that can spontaneously self-assemble into ultratiny spheres, tubes, curved sheets, and ultrathin films [9–11]. This study focuses on the fabrication and characterization of polymer-stabilized Au nanoparticles and nanofilms (PANs). One application of the PAN composed nanodevice is in the detection and possible neutralization of viruses and bacteria [12]. The precise properties of the synthesized nanomaterials depend on the reduction of particle size, monodispersity, stability, and surface topology [13–15]. The focus of this study is on gold nanoparticles and nanofilms, which were prepared by a bottom-up green colloidal method and stabilized using gum Arabic (GA), which is a mixture of saccharides and glycoproteins [16–18]. The reason for using this polymer is that GA acts as a non-toxic dispersing agent and mainly prevents the particles from aggregation [19–21] which lends to optimized device performance.

The noble metal (such as gold) displays properties, which are significantly different from those of individual atoms, surfaces, or bulk materials [22, 23]. For example, gold metal is non-luminescent and lacks catalytic activity, whereas gold colloidal nanoparticles (NPs) exhibit visible luminescence and catalytic activity [24, 25], which can be exploited in nanocatalysis due to their large specific surface areas and in electronic devices for non-linear optics [26, 27]. The presence of free moving electrons in their conduction band gives rise to the surface plasmon band which is dependent on particle size [28, 29]. NPs with diameters smaller than 2 nm have their surface plasmon band strongly diminished because of the low electron density in the conduction band [30]. To synthesize these nanoscale metallic gold, a number of methods have been developed over the years. These methods rely on photochemical and chemical reductions, electrochemical methods, and radiolytic methods to prepare nanoscale Au [31–33]. However, one of the major disadvantages is that the Au-NPs aggregate due to the Van der Waals force interactions between Au atoms [34]. These interactions can be minimized through the use of a colloidal chemistry approach [35]. The colloid method displays advantages of formation of ultrafine particle size, high specific surface area, long triple phase boundary, control of composition at molecular scale, high homogeneity, low cost, and ease of preparation [36, 37]. From our current investigation, it can be demonstrated that Au can be formed by reduction of gold trication (Au^{3+}) using ascorbic acid. This reaction is preferred because of its rapid reaction rate, high reproducibility, and its non-toxic property as a reducing agent. The NPs aggregation can be eliminated through the incorporation of GA.

The study has two broad goals: (a) to provide guidance for cost-effective and green synthesis of PANs, which can be used in the diagnosis of cancer (a future paper will discuss Au nanosensor for cancer detection) and, (b) to characterize the synthesized nanomaterials and the mechanisms of formation of the nanoscale Au clusters using state-of-the-art analytical techniques.

Experimental procedures

All solvents and chemicals were purchased from VWR International (West Chester, PA) unless otherwise specified. Double distilled water (Milli-Q) was used in the preparation of the colloids and PANs.

The experimental procedure was split into two sections: (1) fabrication of polymer-stabilized Au nanoparticles and nanofilms; and (2) characterization of their microstructure. The PANs were prepared using green colloidal chemistry, and the colloidal suspension was deposited on the surface of the substrate (such as glass slides or polymer beads). The characterization of PANs was conducted using X-ray powder diffraction (XRD), atomic force microscopy (AFM), scanning and transmission electron microscopy (SEM and TEM), ultraviolet visible spectroscopy (UV–Vis), and light scattering technique (ZetaPALS).

Fabrication procedure of PAN

A green and cost-effective colloidal chemistry approach was applied in the fabrication of the PAN. For the synthesis of PANs, the reducing agent, (ascorbic acid ($C_6H_8O_6$)) and starting materials (hydrogen tetrachloroaurate (III) trihydrate ($HAuCl_4{\cdot}3H_2O$)) were simultaneously double injected into the aqueous solution containing the dispersing agent (GA) to prevent the particle aggregation. In the presence of excess amount of $C_6H_8O_6$, $HAuCl_4$ (acting as the limiting reactant) was completely reduced to Au metal from Au^{3+}, which formed a colloidal suspension in aqueous solution. The reaction was carried out at 60 °C and under high agitation (1,000 rpm) (Fig. 1). The Au colloid was heated until de-hydrolysis of GA was observed ($\sim$85 °C). The reaction mixture was thoroughly rinsed with ultrapure water (25 mL) and absolute ethanol (25 mL), alternatively. Vacuum filtration was undertaken to obtain Au nanoparticles, which were dried at ambient temperature for 12 h.

For the synthesis of Au nanofilms, the above approach was utilized until a colloid was formed. A 50 μL aliquot of the colloid was deposited onto the surface of a substrate to form a thin film, which was allowed to dry at ambient temperature (Fig. 2a).

Characterization of PAN

An Ultima III XRD with copper (Cu) diffractometer and visual XRD Jade 7 software (Rigaku Americas

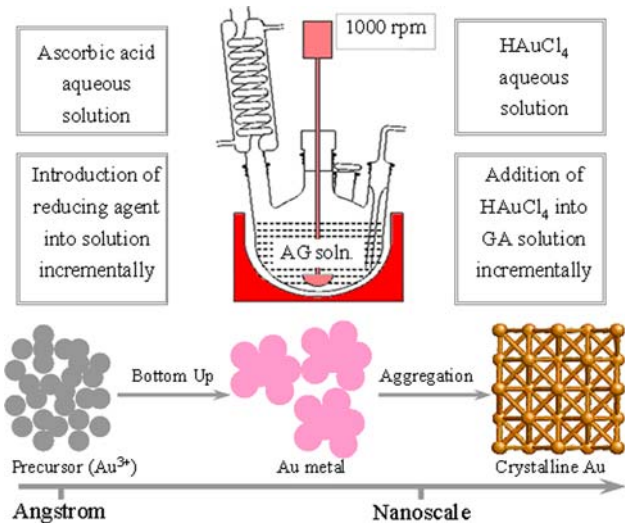

Fig. 1 Nanoscale gold particles derived by green-chemistry method

Incorporation, Houston, TX) was utilized to determine the phase structure and crystalline size. The operating voltage and current were controlled at 40 kV and 44 mA, respectively. A NanoScope IIIa AFM (Veeco Instruments Incorporation, Plainview, NY) was used in taping mode to image the surface topology and roughness of the PAN. To increase the signal-to-noise ratio, the scan rate of 0.587 Hz was applied. The morphology and particle size distribution of the PAN was determined using a Quanta 600 FEG field emission SEM (FEI Company, Hillsboro, Oregon) equipped with X-ray energy dispersive spectrometer (EDS). A field emission gun assembly with Schottky emitter source was used. The voltage was controlled at 5 kV and the beam current at 100 nA. The morphology, particle size distribution, crystallinity, and composition of the PAN were also determined using a Tecnai F20 G^2 TEM (FEI Company, Hillsboro, OH) equipped with EDS and post-column Gatan Image Filter. The PAN particles were dispersed in absolute ethanol and deposited onto the carbon-coated copper grid to prepare the TEM specimen. Magnifications were calibrated using standards of commercial cross-line grating replica and silicon carbide (SiC) to obtain lattice images. The TEM images were taken at a direct magnification of six-hundred thousand magnitudes with the point resolution of 0.2 nm. The chemical composition was determined by EDS. Perkin Elmer Lambda 35 UV–Vis, (PerkinElmer, Fremont, CA) was employed to indentify the Au formation with a scanning range of 200 to 800 nm and concentration of the colloidal suspension of 0.001 M. A ZetaPALS (Brookhaven Instruments Corporation, New York, USA) was employed to measure the particle size distribution and the zeta-potential to evaluate the stability and electrochemical behavior of the Au colloidal suspension. The ZetaPALS utilizes analysis phase light scattering to measure the electrophoretic mobility of charged colloid. The software (ZetaPALS 31311) then converts these

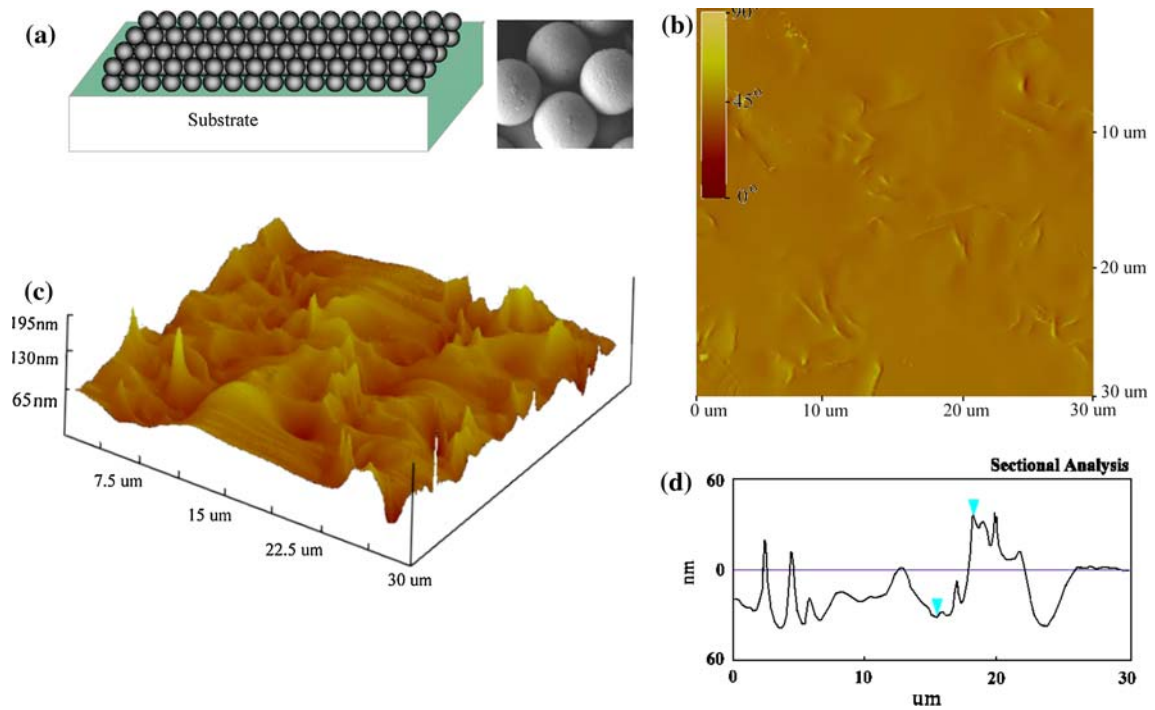

Fig. 2 **a** Simplified diagram of nanoscale gold thin films and Au-coated polymer beads. **b** Topology and height roughness analysis: 2D imaging. **c** Topology and height roughness analysis: 3D imaging. **d** Topology and height roughness analysis: cross-sectional analysis

electrophoretic mobility data to zeta-potential values based on the Smoluchowsky mathematical model.

Results and discussion

Reduction and oxidization (redox) reaction

The redox reaction between tetrachloroaurate (III) trihydrate ($HAuCl_4{\cdot}3H_2O$) and (R)-3,4-dihydroxy-5-(S)-1,2-dihydroxyethyl)furan-2(5H)-one (ascorbic acid, $C_6H_8O_6$) is shown in the following Eq. 1 and 2. The Au^{3+} in the $AuCl_4^-$ complex ions was reduced to Au^0, by ascorbic acid (also known as vitamin C), a bio-reducing species which in turn was oxidized. The following equations are the half redox reaction and its associated standard reduction potential.

$$HAuCl_4(aq) + 3e^- \rightarrow Au^{\circ}(s) + H^+(aq) + 4Cl^-(aq) \quad E^{\circ} = +0.99\,V \tag{1}$$

$$C_6H_8O_6(aq) + 2e^- \rightarrow C_6H_6O_6(aq) + 2H^+(aq) \quad E^{\circ} = +0.06\,V \tag{2}$$

According to these standard reduction potentials of the two half reactions, the overall reaction is determined to have a potential of 0.93 V, which indicates that the redox reaction between $HAuCl_4$ and $C_6H_8O_6$ occurs spontaneously. The released proton from reaction (1) was responsible for the resulting decrease in the pH.

AFM analysis of PAN

The 2D, 3D images, and cross-sectional analysis of the PAN are shown in Fig. 2b–d, respectively. The AFM results of both surface texture and surface cross-sectional measurement indicates that a distinguished grain boundary and well-developed reticulate were formed. The compact and uniform film shows the presence of smooth-terrace feature (2D) formed by polycrystalline particles, with areas averaging approximately 2 μm by 2 μm. The quantitative parameters of average surface roughness (R_a) of 8.74 nm and root-mean-square (R_q) roughness of 19.92 nm were obtained over this scan area. The surface distance was noted to be 2.82 μm, and the horizontal distance 2.81 μm, respectively. The vertical distance, which represents the uniformity of the PAN, was determined to be 64.45 nm. From cross-sectional analysis results, it is demonstrated that the distance between the crest and trough of the Au ultrathin film is approximately 43.22 nm, which indicates that a uniform nanoscale thin film was obtained.

XRD analysis of PAN

XRD was used in providing fingerprint analysis for the PANs crystal structures. The spectrum was obtained at fixed incident beam and detector direction to receive specific reflexing of specimen. Figure 3 displays the XRD spectra of two representative nanopowders, which were prepared under the same variables to confirm the reproducibility of the synthetic method utilized. The XRD spectra aligned well with that of standard face-centered cubic (fcc) Au structure (Jade database PDF No. 000-04-0784, $a = 0.40788$ nm), with the frequency of merit (FOM) of 0.19. This extremely low FOM indicated that the samples are highly crystalline and well correspond with the standard. The average crystallite size (strictly coherence length) was calculated to be approximately 20–30 nm

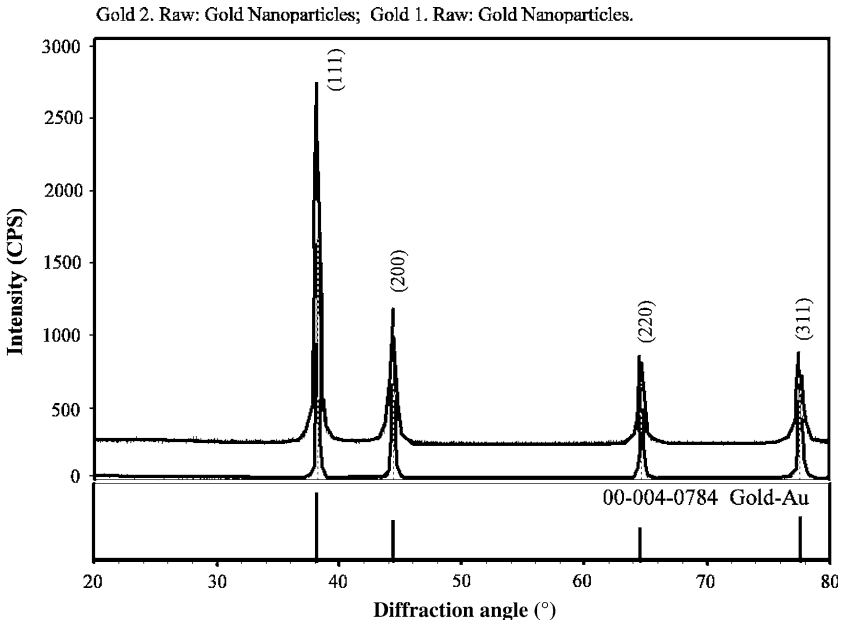

Fig. 3 XRD diffraction of Au metal derived from colloidal chemistry (two specimens shown)

Table 1 The crystallite size of various specimens calculated using the Scherrer equation

# of samples	Crystallite size of (111) plane (nm)	TEM average particle size (nm)	Crystalline index
1	25.72	22.96	1.12
2	28.64	17.67	1.62
3	19.81	18.69	1.06
4	22.54	21.47	1.05
5	23.10	19.91	1.16
6	20.44	19.28	1.06
7	23.54	19.45	1.21
8	26.85	23.15	1.38
9	24.36	21.00	1.16
10	25.79	20.15	1.28
11	28.02	19.19	1.46
12	23.45	19.54	1.20
13	24.67	20.91	1.18
14	27.06	20.04	1.35
15	20.15	19.19	1.05
16	24.32	19.30	1.26
17	27.99	18.91	1.48
18	19.89	18.94	1.05
19	22.46	21.60	1.04
20	24.65	19.88	1.24
21	23.10	20.09	1.15
22	26.43	19.87	1.33
23	21.53	20.50	1.05
24	22.61	21.74	1.04
25	27.68	18.58	1.49
26	22.89	21.59	1.06
27	25.60	21.16	1.21
28	22.92	19.43	1.18

(Table 1) for plane (111) using full width at half maximum (FWHM) using the Scherrer Eq. 3.

$$D_{hkl} = \frac{k\lambda}{\beta \cos\theta} \tag{3}$$

where D is the crystallite size (nm), k is a dimensionless constant of 0.9 for spherical particles, λ is the characteristic wavelength of copper $K_{\alpha 1}$ (0.15418 nm), β is the full width at half maximum (rad), and θ is the diffraction angle (°). The crystallinity (or dimensionless crystalline index) of various specimens was 1.20–1.60 compared with the average size obtained from SEM or TEM analysis using Eq. 4,

$$I_{\text{cry}} = \frac{D_{hkl}(\text{XRD})}{D_{\text{p}}(\text{SEM, TEM})} \tag{4}$$

where I_{cry} is the crystallinity, D_{hkl} is the crystallite size determined using XRD, and D_{p} is the particle size determined from SEM or TEM images.

SEM and TEM analysis of PAN

SEM image (Fig. 4) shows that nanoparticles of PAN are semi-spherical and their sizes are controlled within the range of 20 to 30 nm. The particles viewed under the 10,000 magnification indicate that the particles are distributed uniformly. It was noted that the particles aggregated and were composed of polycrystals with size ranging from 20 to 30 nm, which is consistent with the XRD results (see section "XRD analysis of PAN"). The particle aggregation occurred due to the high surface energy of the nanostructured Au polycrystals which were formed upon heat treatment, noting that the GA was not present. The elemental mapping (Fig. 4 inset) indicates that the Au nanoparticles are distributed on the surface of the substrate evenly.

The morphological and elemental studies through higher resolution (HR) TEM technique are shown in Figs. 5 and 6. HRTEM was used as a complementary technique to SEM, which revealed that mono-dispersed and highly crystalline Au NPs were obtained. The Au NPs appearance is near-spherical with the average particle size from 15 to 20 nm in diameter. The high-resolution image shows that the lattice fringe was distinguishable, which also confirms the formation of Au crystals. It can also be concluded that PAN is highly crystalline from the ring pattern that results from the polycrystals (insets in Fig. 5). The ring pattern of the PAN indicated that the Au was well indexed with the standard metallic pattern, which correlates with the XRD analysis.

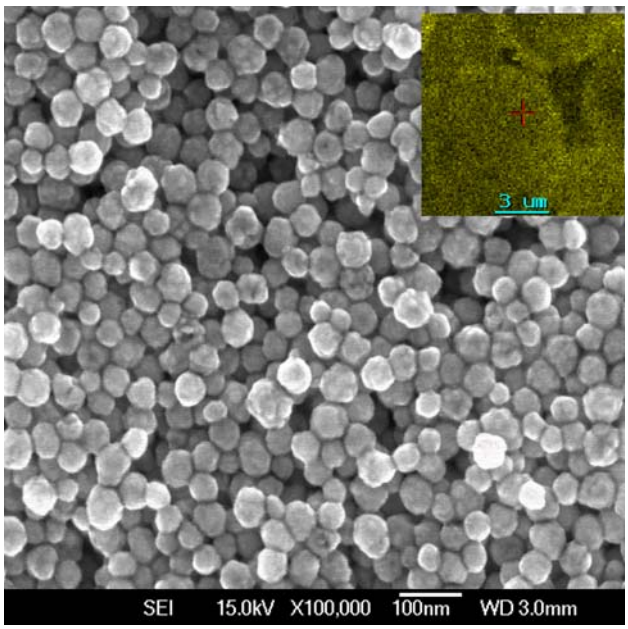

Fig. 4 *main panel* SEM morphology study of PAN ((*inset*) EDS element composition study of PAN with scale bar (note "+" designated center of sample))

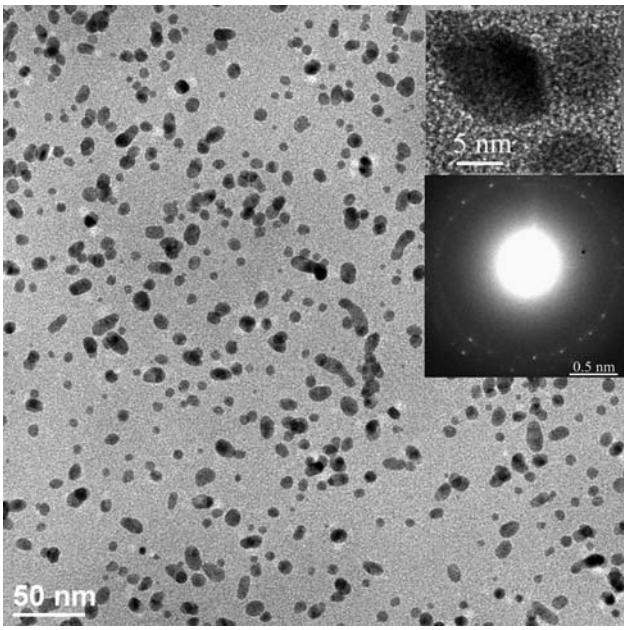

Fig. 5 *main panel* TEM images of gold nanoparticles (*top inset*) lattice fringe ring patterns (*bottom inset*) shown in the *inset*

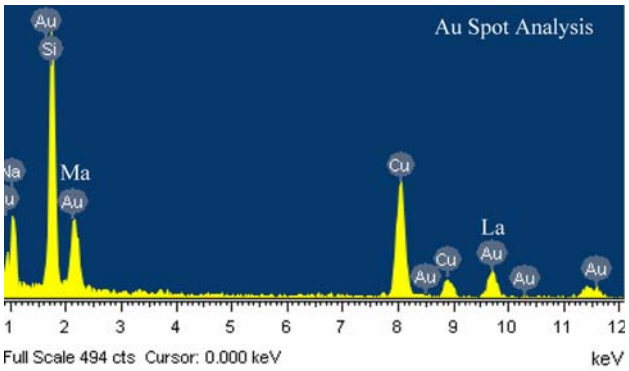

Fig. 6 EDS elemental composition of gold nanoparticles (Cu is from the copper grid)

The EDS spectra of the PAN (Fig. 6) indicated the presence of the Au and Cu elements, noting that metallic Au displays two major peaks of L_α at 9.71 and M_α 2.12 keV, respectively. The other characteristic peaks of PAN were obtained, and correlated to the K_α peak which occurred at 2.10 KeV and the K_β peak which occurred at 2.18 KeV, respectively. The element Cu detected originates from the sample holder used in this experiment (data not shown).

UV–Vis analysis of PAN

UV–Vis spectra confirmed the Au NP formation. The absorbance band detected at *ca.* 550 nm is the characteristic gold surface plasmon peak. From the UV–Vis spectra (Fig. 7), it is observed that during the early stage of the

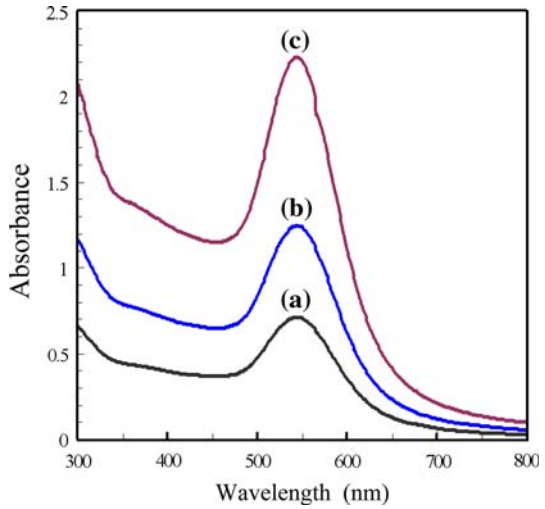

Fig. 7 UV–Vis of Au colloidal dispersion. The spectra was taken at different times of the reaction. (*a*) 5 min, (*b*) 10 min, (*c*) 20 min

redox reaction, the number of gold particles increases and a limited aggregation is observed until the procedure is terminated. This result was also in good agreement with our primary studies on silver nanoparticles [38]. The plasmon characteristic peak at approximately 550 nm indicated that metallic gold particles were formed. This observation is confirmed by the XRD analysis, which also indicated that the metallic gold was obtained using colloidal chemistry redox reaction.

Particle size and electrokinetics of PAN

In order to evaluate the stability and electrokinetic behavior of the PAN colloid, the zeta-potential (also known as effective surface potential, denoted as ζ) was measured by imposing an electrical field (20 mV) across the colloid particles. The measured ζ allows an estimation of the degree of aggregation. It is commonly agreed that the fine particles have high surface tension during the fabrication procedure and large absolute zeta-potential. The particle size distribution and zeta-potential analysis of Au colloidal suspension is summarized graphically (Figs. 8, 9, 10). The particle size is ranging from *ca.* 10 to 15 nm (Fig. 8). This observation is different from the XRD and TEM/SEM studies, which indicates that the aggregation occurs after de-hydrolysis of GA (the dispersing agent) at 85 °C. After removal of GA, the Au cluster aggregates due to its high surface energy (Fig. 9). It was also found that the zeta-potential essentially ranges from −40 to −45 mV (Fig. 10), which depends on the particle sizes of the PAN. The magnitude of the measured zeta-potential indicates the high stability of the colloid. The particles with large absolute zeta-potential (arising from negatively charged particles) were able to minimize their aggregation due to

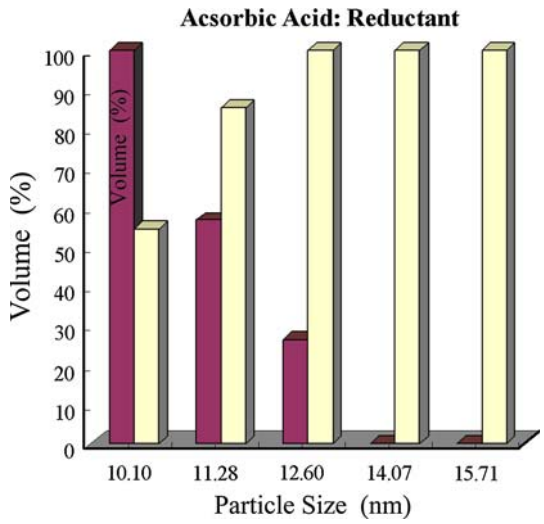

Fig. 8 Particle size distribution of Au colloid

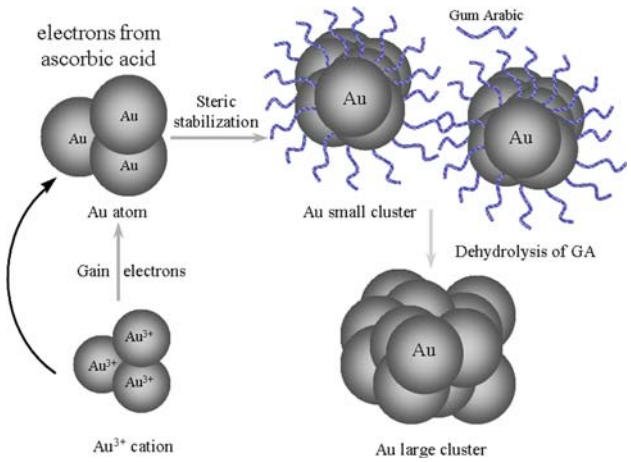

Fig. 9 Mechanism of gold formation and its aggregation

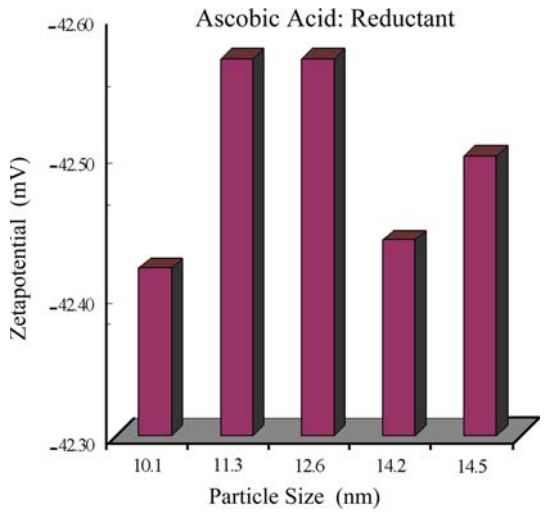

Fig. 10 Measured zeta potential of Au colloid

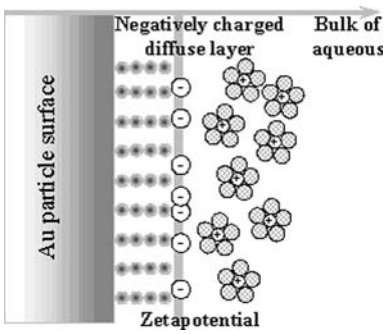

Fig. 11 Schematic of zeta potential study

electrostatic repulsion. The particle interaction and double layer formation is shown schematically (Fig. 11). From the schematic, it can be observed that the zeta-potential corresponds to the electric potential at the conceptual diffusion layer, which is negatively charged. If this electric potential exhibits high absolute magnitude value, the repulsion between particles exceeds the van der Waals long-range attractive forces, and fine particles will be formed. When the zeta-potential approaches zero, particles tend to aggregate when the GA is absent, due to de-hydrolysis. Under these conditions, the van der Waals attraction exceeds the electrostatic repulsion; therefore, the Au particles tend to agglomerate.

Conclusions

The polymer-stabilized Au nanoparticles and nanofilms (PANs) were developed using cost-effective green colloidal chemistry and evaluated using advanced instrumentation techniques. The gold nanoparticles (NPs) were indexed with cubic crystalline phase structure from XRD analysis. AFM indicates that gold nanofilms were highly uniform (*ca.* 43 nm in thickness), with the relative standard deviation (RSD) of 19.92 nm. It was also concluded from the SEM and TEM studies that the green synthesized nanomaterials were composed of near-spherical particles. The average particle size was 11.3 nm (100%) and 12.6 nm (relative to the most abundant peak at 98%) from ZetaPALS analysis, whereas the XRD calculation and SEM images indicated that the particles size was approximately 25 nm. The limited degree of aggregation may be attributed to dehydrolysis of GA, where the van der Waals attractive forces are less than the electrostatic repulsive force with specific zeta-potential (*ca.*−42.50 mV). The zeta-potential in turn depends upon particle size.

Acknowledgements The Academia Mexicana de Ciencias (AMC) y Fundación México Estados Unidos para la Ciencia (FUMEC), and the College of Arts and Sciences at Texas A&M University-Kingsville (TAMUK), Research and Development Fund (RDF) are duly

acknowledged for their financial assistance. The authors are also grateful for the technical support and facility access provided by the South Texas Environmental Institute, the Department of Chemistry at TAMUK, and the Microscope and Imaging Center and Materials Characterization Facility at Texas A&M University, College Station.

References

1. Sokolov K, Nida D, Descour M, Lacy A, Levy M, Hall B, Dharmawardhane S, Ellington A, Korgel B, Richards-Kortum R (2007) Adv Cancer Res 96:299
2. Kelsall R, Hamley IW, Geoghegan M (2005) Nanoscale science and technology. Wiley, New Jersey
3. Drexler E, Peterson C, Pergamit G (1991) Unbounding the future: the nanotechnology revolution. William Morrow and Company, New York
4. Drexler KE (1990) Engines of creation: the coming era of nanotechnology. Bantam Dell Publishing Group Inc (Random House), New York
5. Drexler KE (1992) Nanosystems: molecular machinery, manufacturing, and computation. Wiley, New Jersey
6. Wang ZL (2003) Nanowires and nanobelts materials, properties and devices nanowires and nanobelts of functional materials (I). Kluwer Academic Publishers, Norwell
7. Weiss PS, Lewis PA (2007) ACS Nano 1:145
8. Vauthey S, Santoso S, Gong H, Watson N, Zhang S (2002) Biophysics 16:5355
9. Csáki A, Möller R, Straube W, Köhler JM, Fritzschea W (2001) Nucleic Acids Res 16:1
10. Garzoń IL, Artacho E, Beltrań MR, Garćia A, Junquera J, Michaelian K, Ordejoń P, Rovira C, Sanchez-Portaĺ D, Soler JM (2001) Nanotechnology 12:126
11. Chen CS (2008) Nat Nanotechnol 3:13
12. Li Z, Jin R, Mirkin CA, Letsinger RL (2002) Nucleic Acids Res 30:1558
13. Rosi NL, Giljohann DA, Thaxton CS, Lytton-Jean AKR, Han MS, Mirkin CA (2006) Science 312:1027
14. Chen K, Adelstein SJ, Kassis AI (2004) J Mol Struct Theochem 711:49
15. Glomm WR (2005) J Dispers Sci Technol 26:389
16. Lévy R, Thanh NTK, Doty RC, Hussain I, Nichols RJ, Schiffrin DJ, Brust M, Fernig DG (2004) J Am Chem Soc 126:10076
17. Dougan JA, Karlsson C, Smith WE, Graham D (2007) Nucleic Acids Res 35:3668
18. Yan JF, Liu J (2008) Nanomed Nanotechnol Biol Med 4:79
19. Opdahl A, Petrovykh DY, Kimura-Suda H, Tarlov MJ, Whitman LJ (2007) PNAS 104:9
20. Vo-Dinh T, Kasili P, Wabuyele M (2006) Nanomed Nanotechnol Biol Med 2:22
21. Zhang S, Metelev V, Tabatadze D, Zamecnik PC, Bogdanov A Jr (2008) PNAS 105:4156
22. Teicher BA (2002) Tumor models in cancer research (Cancer drug discovery and development). Humana Press Inc, New Jersey
23. Shacham R, Avnir D, Mandler D (1999) Adv Mater 11:384
24. Fan H, Yang K, Boye DM, Sigmon T, Malloy KJ, Xu H, López GP, Brinker CJ (2004) Science 304:567
25. Sánchez-Loredo MG, Robledo-Cabreraa A, Groteb M (2002) Materi Chem Phys 76:279
26. Sambrook J, Russell D (2001) Molecular cloning: a laboratory manual. Cold Spring Harbor Laboratory Press, Cold Spring Harbor
27. Ciccolini LS, Ayazi Shamlou P, Titchener-Hooker NJ, Ward JM, Dunnill P (2000) Biotechnol Bioeng 60:768
28. Weller MT (1994) The application and interpretation of powder X-ray diffraction data, in inorganic materials chemistry. Oxford University Press, New York
29. Garratt-Reed AJ, Bell DC (2003) Energy dispersive X-ray analysis in the electron microscope. BIOS Scientific Publisher Limited, Oxford
30. Tanev S, Pond J, Paddon P, Tuchin VV (2006) A finite-difference time-domain model of optical phase contrast microscope imaging (Optical waveguide sensing and imaging). Springer, Netherlands
31. Stokes RJ, Macaskill A, Lundahl PJ, Smith WE, Faulds K, Graham D (2008) Small 3:1593
32. Massa W (2004) Crystal structure determination. Springer, Berlin
33. Kline R (2004) Principles and practice of structural equation modeling (Methodology in the social sciences). Guilford Publications Inc, New York
34. Inaga S, Osatake H, Tanaka K (1991) J Electron Microsc 40:181
35. Hobot J, Walker M, Newman G, Bowler P (2008) J Electron Microsc 57:67
36. Kneipp K, Haka AS, Kneipp H, Badizadegan K, Yoshizawa N, Boone C, Shafer-Peltier KE, Motz JT, Dasari RR, Feld MS (2002) Appl Spectrosc 56:150
37. Firkowska I, Giannona S, Rojas-Chapana JA, Luecke K, Brüstle O, Giersig M (2008) Biocompatible nanomaterials and nanodevices promising for biomedical applications, (Nanomaterials for application in medicine and biology). Springer, Netherlands
38. Medina-Ramírez I, Bashir S, Luo Z, Liu J (2009) Colloids Surf B Biointerfaces 73:185